COVID-19 transmission inside a small passenger vessel: Risks and mitigation

Ocean Engineering 255 (2022) 111486

Contents lists available at ScienceDirect

Ocean Engineering

journal homepage: www.elsevier.com/locate/oceaneng

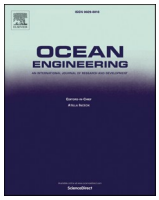

COVID-19 transmission inside a small passenger vessel: Risks and mitigation

Luofeng Huang [a,b,*], Soegeng Riyadi [c], I.K.A.P. Utama [c], Minghao Li [d], Peiyign Sun [e], Giles Thomas [b]

[a] School of Water, Energy and Environment, Cranfield University, UK
[b] Department of Mechanical Engineering, University College London, UK
[c] Department of Naval Architecture, Institut Teknologi Sepuluh Nopember, Indonesia
[d] Department of Mechanics and Maritime Sciences, Chalmers University of Technology, Sweden
[e] School of Engineering and Informatics, University of Sussex, UK

ARTICLE INFO

Keywords:
COVID-19
Passenger vessel
Virus
Airborne transmission
Computational fluid dynamics
Particle modelling

ABSTRACT

The global shipping industry has been severely influenced by the COVID-19 pandemic; in particular, a significant amount of passenger transportation has been suspended due to the concern of COVID-19 outbreak, as such voyages confine a dense crowd in a compact space. In order to accelerate the recovery of the maritime business and minimise passengers' risk of being infected, this work has developed a computational model to study the airborne transmission of COVID-19 viruses in the superstructure of a full-scale passenger vessel. Considering the vessel advancing in open water, simulations were conducted to study the particulate flow due to an infected person coughing and speaking, with the forward door open and closed. The results suggest that keeping the forward door closed will help prevent the external wind flow spreading the virus. When the forward door is closed, virus particles' coverage is shown to be limited to a radius of half a metre, less than a seat's width. Thus, an alternate seat arrangement is suggested. Furthermore, investigations were conducted on the influence of wall-mounted Air Conditioner (AC) on the virus transmission, and it was found that controlling the AC outlet direction at less than 15° downward can effectively limit the virus spread. Meanwhile, it was demonstrated that an AC's backflow tends to gather virus particles in a nearby area, thus sitting farther from an opening AC may reduce the risk of being infected. Overall, this work is expected to inform hygienic guidelines for operators to counter COVID-19 and potentially similar viruses in the future.

1. Introduction

The maritime industry has been severely affected by the COVID-19 pandemic. Ships are currently operating with reduced capacity or restricted from leaving port. In particular, the operation of passenger vessels has been reduced by up to 42.77% (Millefiori et al., 2021). Crew and passengers can be exposed to a serious risk of contagion, since the compact and crowded space of ships implies a high likelihood of COVID-19 outbreak. In this context, there is an urgent need to research the best technical solutions to ensure COVID-19 safety for ships (Thomas et al., 2021).

COVID-19 infection has been found to be primarily induced by inhalation (Jin et al., 2020). The virus can be transmitted via air, existing in a form of aerosols and droplets injected by humans coughing, speaking, breathing, singing and sneezing (Vuorinen et al., 2020). Coughing and speaking are the most likely scenarios, as coughing is one of the primary COVID-19 symptoms whilst speaking is almost inevitable in daily contacts and can actually output a significant amount of the virus (Chao et al., 2009). The transmission mechanism of the COVID-19 virus may be referred to in previous work that studied flu, as it has a similar mechanism to SARS (Gao and Niu, 2007).

To investigate the airborne transmission of COVID-19 virus, Computational Fluid Dynamics (CFD) has the capability to understand the virus's movement and coverage, which is essential for developing effective mitigation strategies for infection control. To date, computational studies of COVID-19 transmission have been conducted for certain high-risk areas. For example, Zhang et al. (2021a) performed a CFD analysis for virus transmission inside a bus. A simple air-spray

* Corresponding author. School of Water, Energy and Environment, Cranfield University, UK.
E-mail address: luofeng.huang@cranfield.ac.uk (L. Huang).

https://doi.org/10.1016/j.oceaneng.2022.111486
Received 10 February 2022; Received in revised form 26 April 2022; Accepted 4 May 2022
Available online 8 May 2022

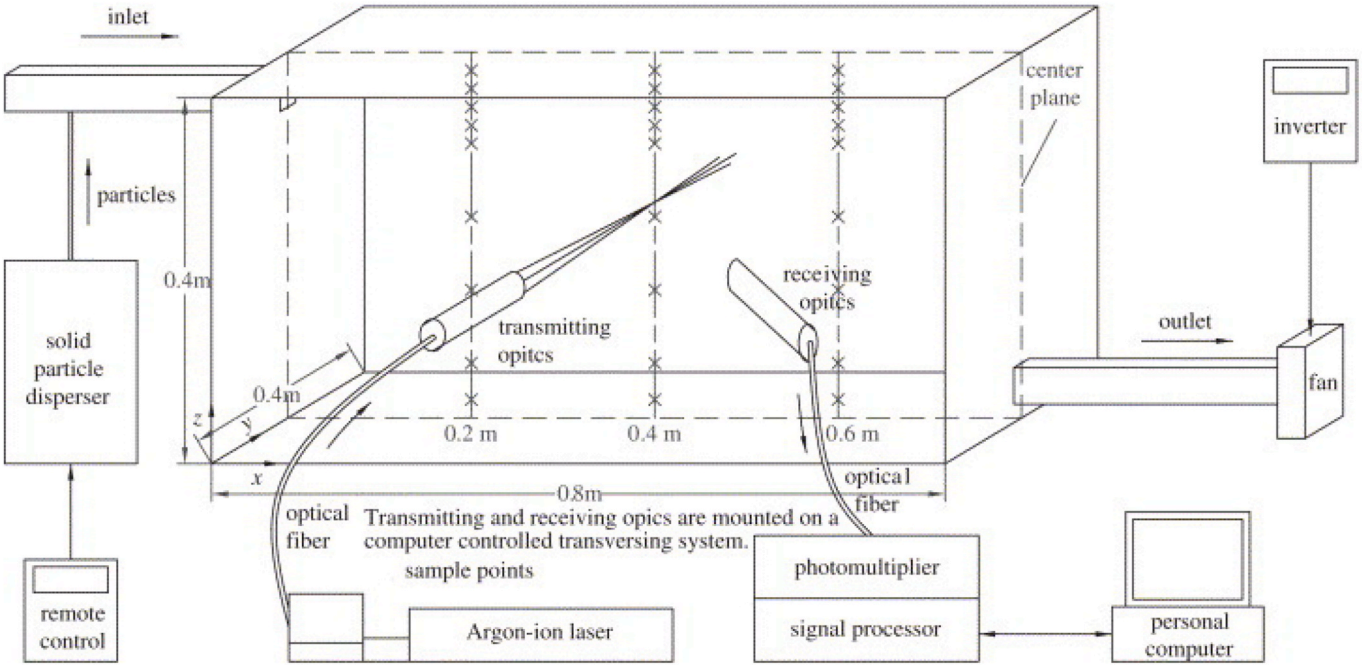

Fig. 1. Experimental setup of Chen et al. (2006).

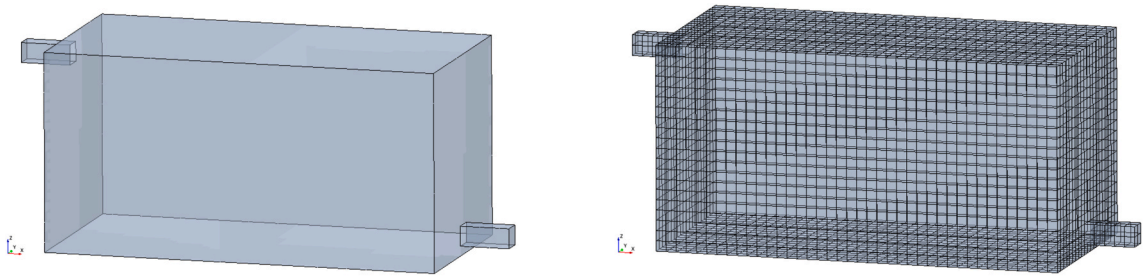

(a) Computational domain (b) Discritised computational domain

Fig. 2. Computational model to repeat the experiment of Chen et al. (2006).

experiment was also conducted to validate the CFD model (Zhang et al., 2021b). They compared the validated CFD results with the prediction from an analytical approach that was previously widely used. The comparison indicates that the analytical approach produces significant inaccuracies due to a lack of consideration of complex velocity and particle concentration fields. Thus they suggest that CFD should be used in future studies. Abuhegazy et al. (2020) and Talaat et al. (2021) used CFD to investigate the virus transmission in, respectively, a classroom and a passenger aeroplane; both papers suggest placing lateral shields/barriers between people sitting side-by-side, with simulations used to demonstrate their effectiveness. Guo et al. (2021) used CFD to study the virus transmission in hospital rooms. As the central AC system in hospitals may cause extensive spreading of the virus, they suggested placing portable air purifiers for mitigation and used simulations to identify the ideal locations for air purifiers. Welch et al. (2022) used CFD to demonstrate the effectiveness of using ultraviolet lights to limit the virus' airborne transmission.

Based on the above review, CFD has become a standard approach to studying COVID-19's airborne transmission in various scenarios. However, relevant research has not been seen for scenarios on board ships. During ship operations, natural winds, ACs and ventilation systems can induce airborne transmission of virus particles inside a vessel. The airflow environment on ships is unique due to its forward motion and the location of a doorway facing forward at the front of the passenger area which can be open. This open door may allow a significant wind flow in the passenger area when the ship is moving. In addition, relatively small ships usually use wall-mounted ACs instead of a central AC system. The airflow direction of the wall-mounted ACs can be adjusted, and the influence on COVID-19 transmission should be studied.

In this context, the present work develops a CFD-based model to analyse the potential transmission of the COVID-19 virus inside a ship. The paper starts by introducing the theories and practicalities of the model, followed by validating the model against experimental measurements of velocity field and particle diffusion inside an idealised room. Subsequently, the room geometry was replaced by the superstructure of a small passenger ship. Analyses were presented on the virus distribution in different scenarios, concerning a passenger coughing or speaking when the vessel's forward door is open or closed, and investigating the influence of AC winds on the virus spread. The obtained results were used to discuss measures that may minimise the spread and contagion risk of COVID-19 virus.

2. Computational approach

CFD is used to model airflow whilst the transmission of virus particles is tracked by a Lagrangian approach. The simulations were

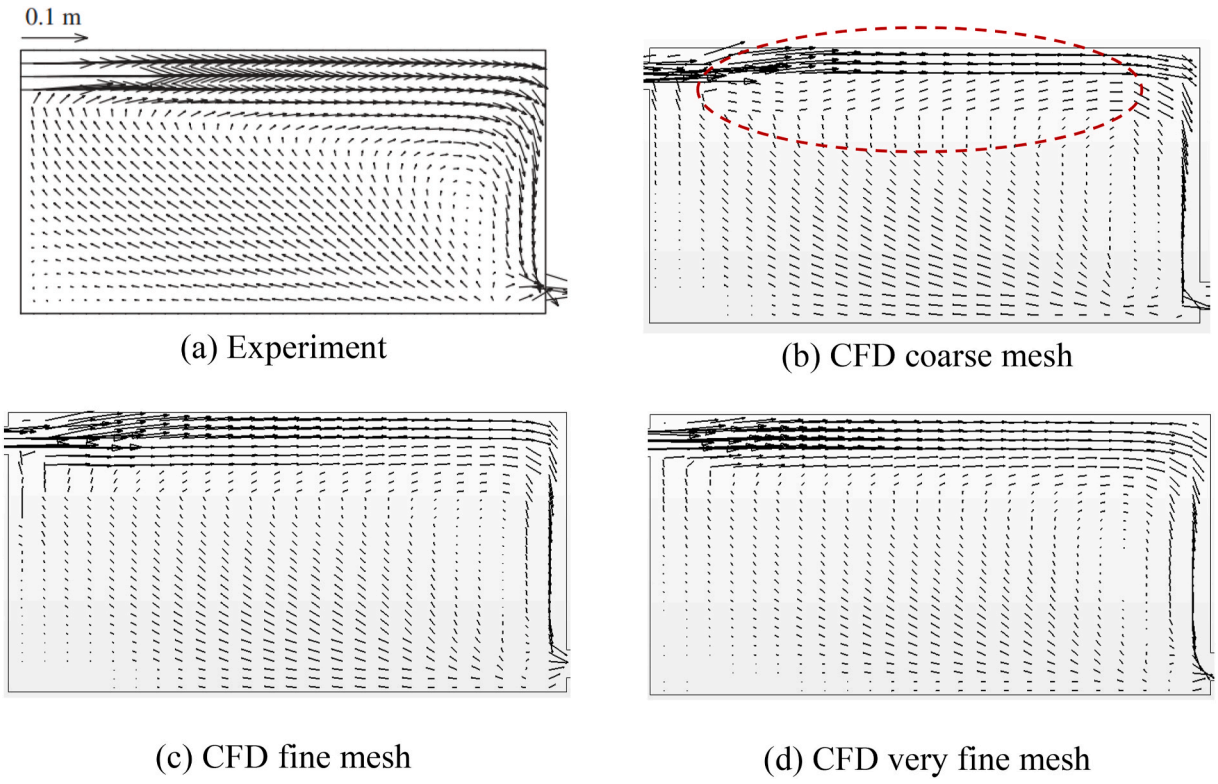

Fig. 3. Experimental and computational results of velocity field.

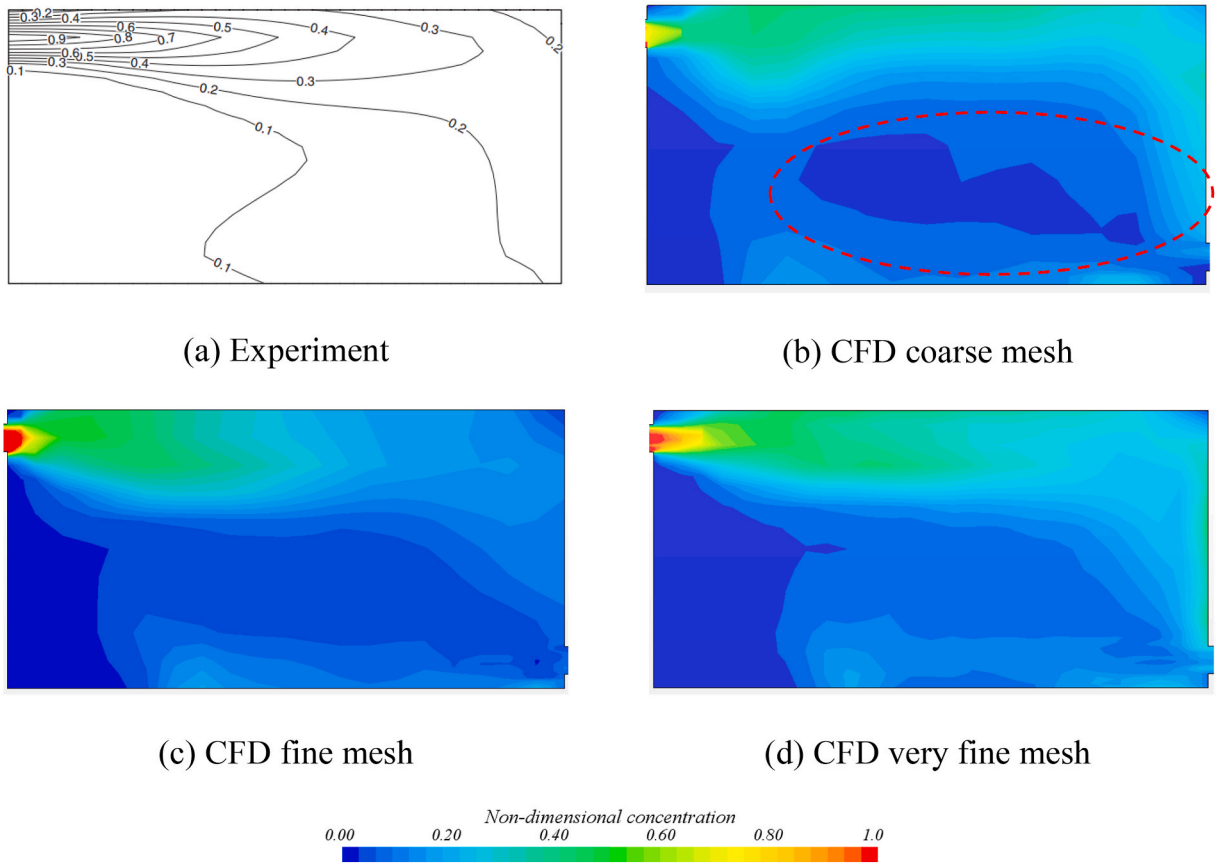

Fig. 4. Experimental and computational results of particle concentration.

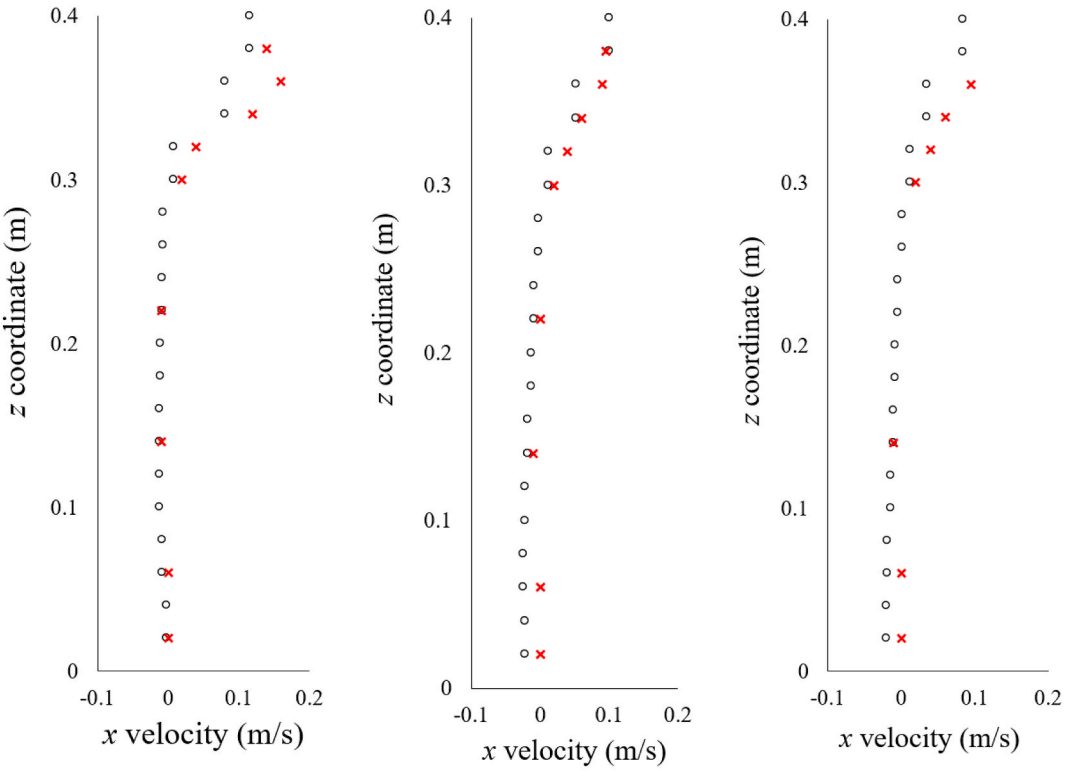

(a) $x = 0.2$ m (b) $x = 0.4$ m (c) $x = 0.6$ m

Fig. 5. Quantitive comparison of velocity measured at certain locations of the central plane: experiment (red crosses) and CFD fine mesh (black circles). (For interpretation of the references to colour in this figure legend, the reader is referred to the Web version of this article.)

Fig. 6. A passenger ship operated by PT. Pelayaran Nasional Ekalya Purnamasari (PNEP).

performed using the commercial software STAR-CCM+.

2.1. Governing equations

In this work, Lagrangian particles are applied to model the COVID-19 virus aerosols/droplets, by which the particle movement is subjected to its gravity ($\boldsymbol{G}$) and a drag force from its surrounding airflow ($\boldsymbol{F_d}$):

$$m\frac{\mathrm{d}\overline{V_P}}{\mathrm{dt}} = \boldsymbol{G} + \boldsymbol{F}_d \tag{1}$$

where m denotes the particle's mass, $\overline{V_P}$ is the particle's velocity, $\boldsymbol{G} = m\boldsymbol{g}$ and g is set at 9.81 m/s^2. The fluid drag force is calculated through the Schiller-Naumann Correlation (Liu et al., 1993):

$$\boldsymbol{F_d} = \frac{1}{2}C_d\rho_P A_P|V_s|\,V_s \tag{2}$$

where ρ_P is the particle density, A_P is the particle project area and V_s is the relative velocity between the particle and the air. C_d is an empirical coefficient calculated based on the particle's Reynolds number (Re_P), which is defined as follows.

$$C_d = \begin{cases} \dfrac{24}{Re_P}\left(1 + 0.15Re_P^{0.687}\right), & if\ Re_P \le 1000 \\ 0\,44 \quad , & if\ Re_P > 1000 \end{cases} \tag{3}$$

The surrounding fluid flow is solved by the standard Reynolds-Averaged Navier-Stokes (RANS) equations:

$$\nabla\cdot\overline{\mathbf{v}} = 0 \tag{4}$$

$$\frac{\partial(\rho\overline{\mathbf{v}})}{\partial t} + \nabla\cdot(\rho\overline{\mathbf{v}}\overline{\mathbf{v}}) = -\nabla\overline{p} + \nabla\cdot(\overline{\tau} - \rho\overline{\mathbf{v}'\mathbf{v}'}) + \rho g \tag{5}$$

where $\overline{\mathbf{v}}$ is the time-averaged velocity, $\mathbf{v}'$ is the velocity fluctuation, ρ is the fluid density ($\rho_{\mathrm{air}} = 1$ kg/m^3), $\overline{p}$ denotes the time-averaged pressure, $\overline{\tau} = \mu[\nabla\mathrm{v} + (\nabla\mathrm{v})^{\mathrm{T}}]$ is the viscous stress term, μ is the dynamic viscosity ($\mu_{\mathrm{air}} = 1.48 \times 10^{-5}$ N s/m^2). Since the RANS equations have considered the turbulent fluid, the Shear Stress Transport (SST) k − ω model was adopted to close the equations (Menter, 1993; Pena and Huang, 2021).

In particular, a sufficiently-small particle in turbulent flow reveals a randomly-varying velocity field, which induces the microscopic particles to perform constant stochastic motions thus diffusing. This behaviour is modelled by including the effect of instantaneous velocity fluctuations on the particle (Gosman and Loannides, 1983):

$$\mathbf{v} = \overline{\mathbf{v}} + \mathbf{v}' \tag{6}$$

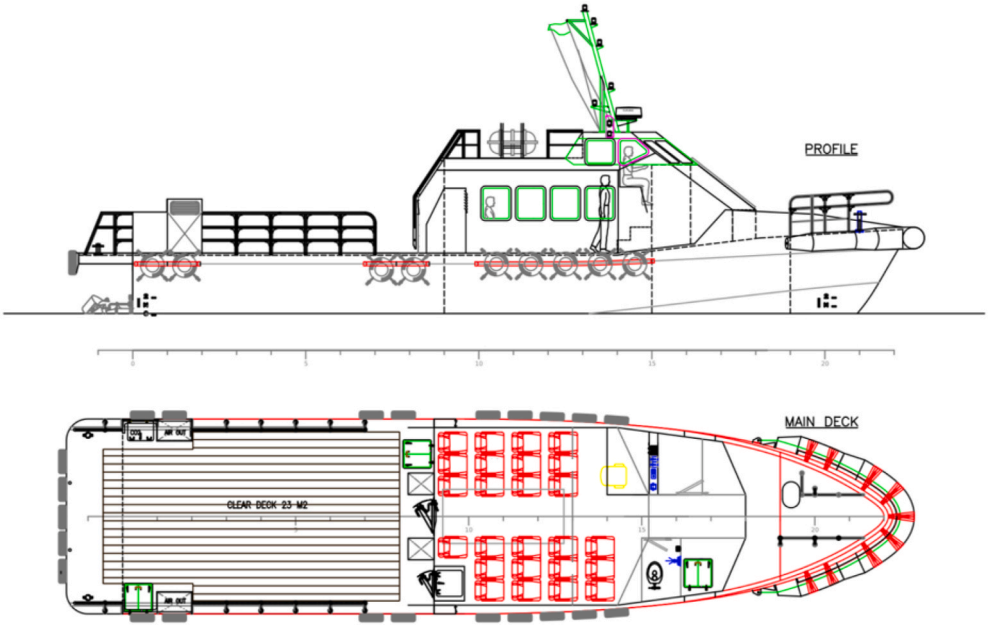

Fig. 7. Profile and plan views of the ship's external and internal design.

Table 1
The details of virus import due to coughing and speaking (Chao et al., 2009).

Virus source	Coughing	Speaking
Injection duration	0.3 s, short event	60 s, long event
Inject speed	11.7 m/s	3.1 m/s
Particle diameter	13.5 μm	16 μm
Inject particle number	6950 per second	443 per second

To be more specific, the applied fluid velocity in calculations is $\mathbf{v}$, which is different from a usual RANS approach for macroscopic problems where $\bar{\mathbf{v}}$ is directly used to simplify the calculation, e.g. (Huang et al., 2020).

2.2. Validation

Based on the above governing equations, a validation study was conducted to reproduce the experiment of Chen et al. (2006). The experiment used artificial particles to mimic a flu virus, which has very similar particle dimensions, airborne transmission mechanism, and infection mechanism to COVID-19 virus. The experiment was conducted in a cubic chamber, with a size of 0.8 m × 0.4 m × 0.4 m, as shown in Fig. 1. The chamber has an air inlet near the left top side and an outlet near the right bottom side. The inlet and outlet sections are of the same size, 0.04 m × 0.04 m. The centers of them are located at x = 0, y = 0.2 m, z = 0.36 m and x = 0.8 m, y = 0.2 m, z = 0.04 m. Particles were injected from the inlet with airflow and diffused in the entire room. The velocity profile and particle distribution were measured across the centre plane of the chamber (the centre plane is marked in Fig. 1).

To reproduce the experiment, a computational domain of the same size, inlet and outlet was established, as shown in Fig. 2(a). The inlet was set as "fixed-velocity inlet" with a constant airflow velocity of (0.225, 0, 0) m/s, and the outlet was set as "fixed-pressure outlet" with a reference pressure of 0 Pa. This value is insignificant since the CFD calculation is based on relative pressure. Other boundaries are "non-slip walls". Spherical Particles of a diameter of 1×10^{-5} m and a density of 1.4×10^{-3} kg/m^3 were injected with the inlet flow, at a rate of 1000 particles per second. The particle concentration at the inlet was used as a non-dimensional standard, denoted as $C_{inlet} = 1$. Initially there is no particle in the domain, i.e. $C_{t=0} = 0$. The particles were set to attach to walls upon contact and can leave the domain from the outlet. The above parameters were set to be consistent with the validation experiment.

The computational domain was then discretised into a hexahedral

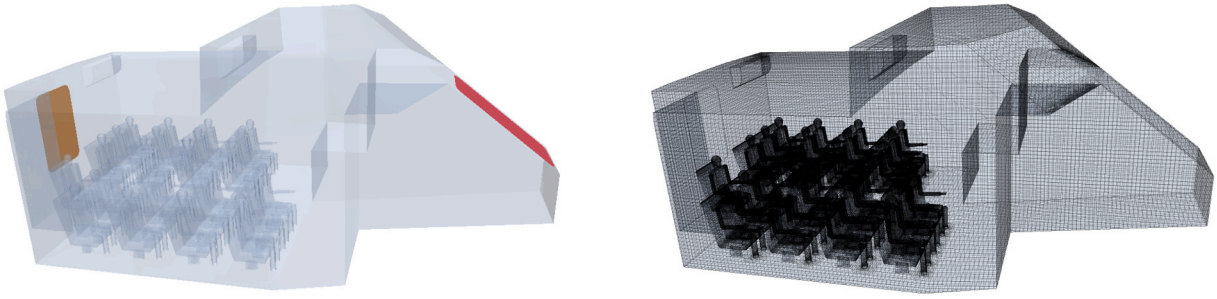

(a) Computational domain with vessel's forward door in red and back door in brown

(b) Discritised computational domain

Fig. 8. Computational model of the vessel's internal space.

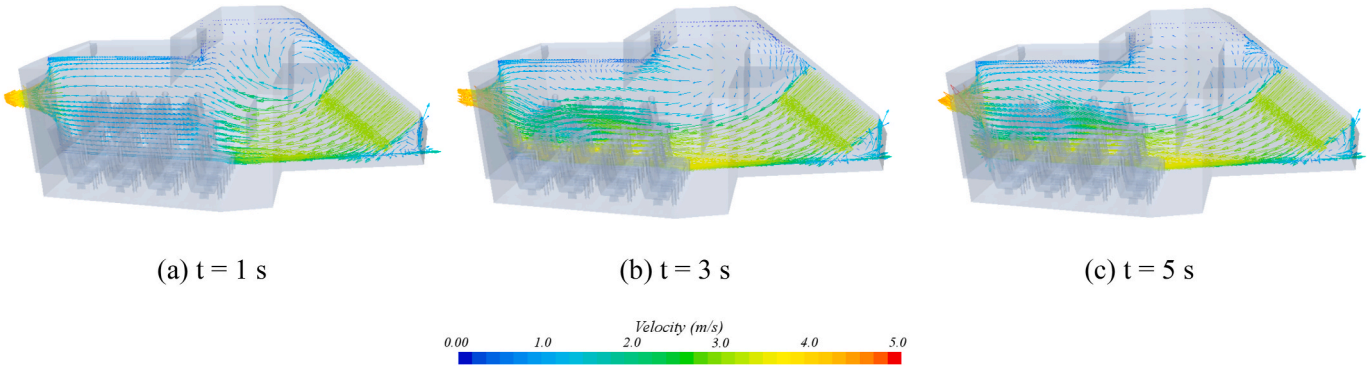

Fig. 9. Velocity field across the centre plane, when V = 6 knots and the forward door is open: the difference between t = 3 s and t = 5 s is negligible, so the flow at t = 5 s is deemed converged.

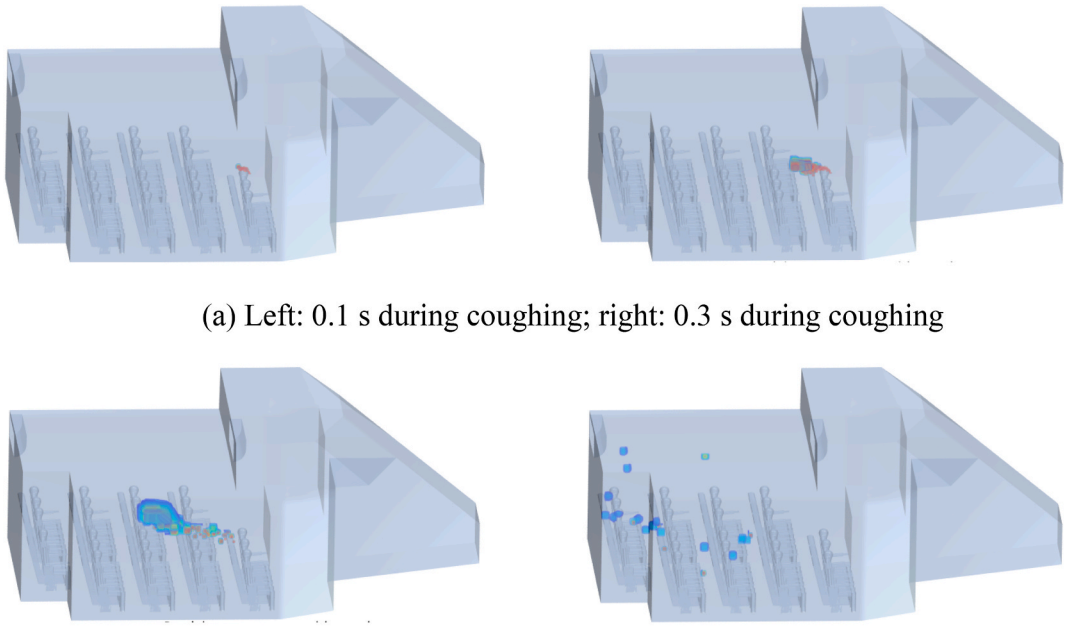

Fig. 10. Coughing with the forward door open.

mesh, as shown in Fig. 2(b). A mesh sensitivity test is presented with three different cell sizes, respectively 0.05 m (coarse), 0.04 m (fine) and 0.03 m (very fine). The three mesh sizes were tested with a maximum Courant number of 1 to determine the corresponding timestep size. Simulations using the three sets of meshes were run for 60 s, and the same measurements as per the experiment were taken for comparison, i.e. the velocity profile and particle distribution were measured across the centre plane of the box. To assess the numerical uncertainty from spatial discretisation, an estimation was conducted as reported in Appendix A. The Grid Convergence Index (GCI) method (Celik et al., 2008) was used and the numerical uncertainty in the fine-grid solution for the fine mesh turned out to be 3.68%.

Figs. 3 and 4 show a qualitative comparison between the experimental measurements and simulations performed with the three mesh densities. Overall there is good consistency between the experiment, CFD with fine mesh, and CFD with very fine mesh. This can be seen in both the velocity and concentration results. However, there are certain inaccuracies in the coarse mesh results, as circled in the figures. Therefore, the fine mesh density was chosen for the following investigations, as it requires less computational recourses than the very fine mesh whilst maintaining the required accuracy.

Furthermore, a quantitive comparison was performed between the experiment and CFD with fine mesh. Specific velocity data measured in the experiment are compared with corresponding CFD results, as plotted in Fig. 5. Good agreement can be seen for all the data points, which confirms the accuracy of the CFD model. Based on the results presented in this section, the present computational approach is deemed suitable to study the airborne transmission of COVID-19 virus.

3. Ship model and COVID-19 risks

Upon validation of the computational approach, a small passenger ship operating in Indonesia was selected as the research object of this paper. The vessel's photo and geometry drawings are shown in Figs. 6

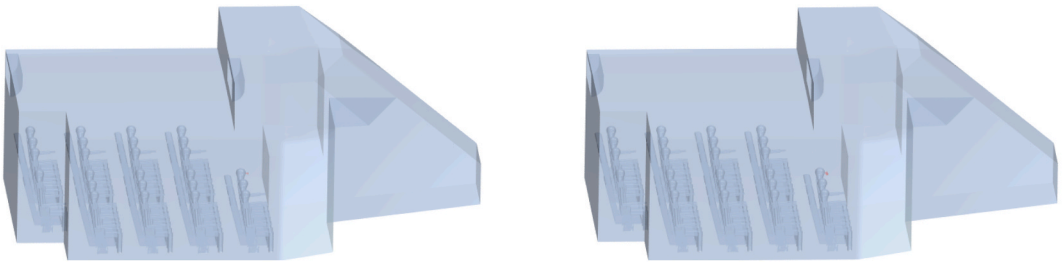

(a) Left: 0.1 s during coughing; right: 0.3 s during coughing

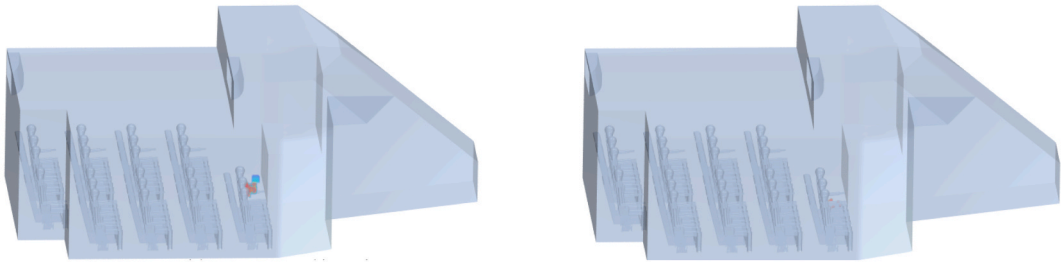

(b) Left: 50 s after coughing; 100 s after coughing

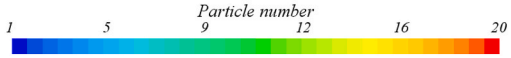

Fig. 11. Coughing with the forward door closed.

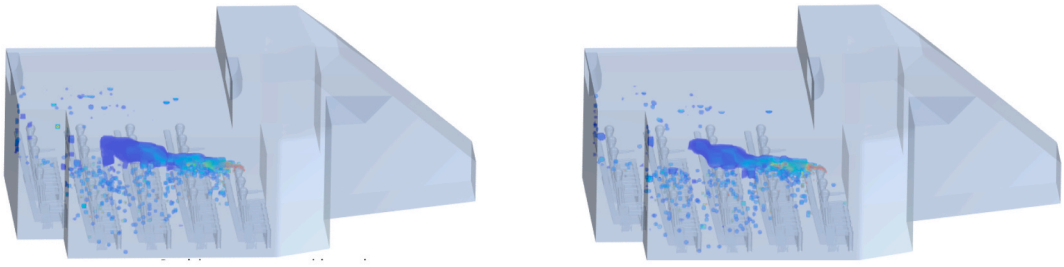

(a) Left: 30 s during speaking; right: 60 s during speaking

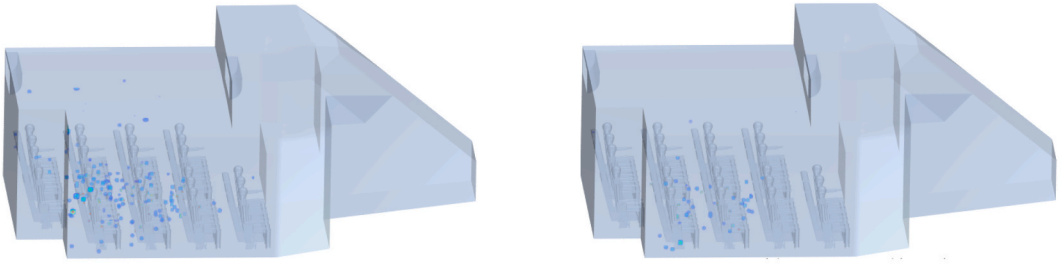

(b) Left: 5 s after speaking; 10 s after speaking

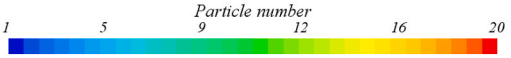

Fig. 12. Speaking with the forward door open.

and 7. It is 19.5 m long and 4.5 m wide, with an internal space of approximately 7 m long that contains 25 seats. This vessel is used to transport workers to and from offshore installations such as drilling platforms. There are two primary reasons for choosing this ship for the present study:

(1) The operation of this vessel type in Indonesia has been significantly impacted ships by COVID-19. The country, heavily reliant

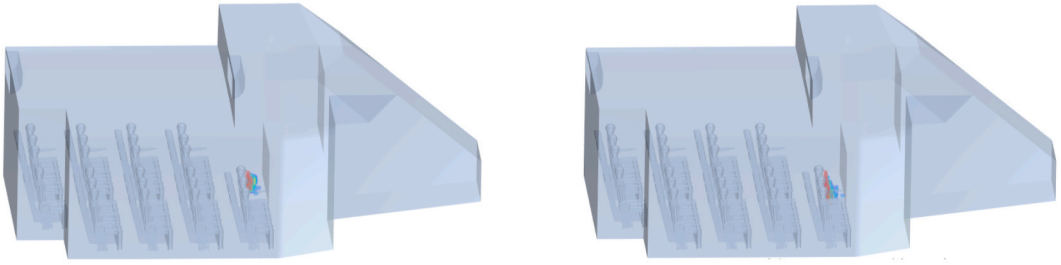

(a) Left: 30 s during speaking; right: 60 s during speaking

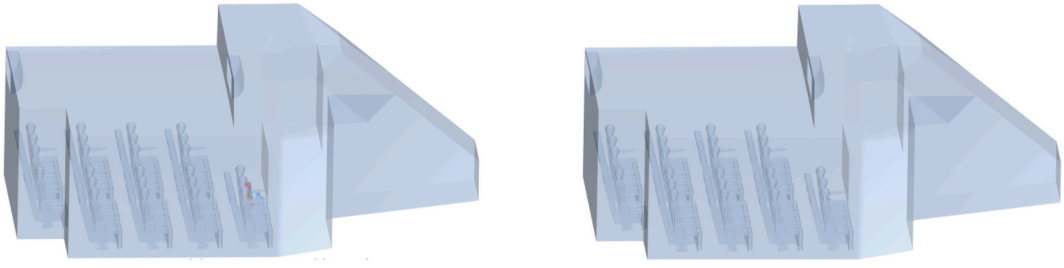

(b) Left: 30 s after speaking; 60 s after speaking

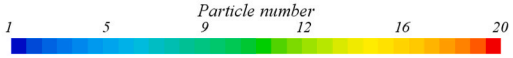

Fig. 13. Speaking with the forward door closed.

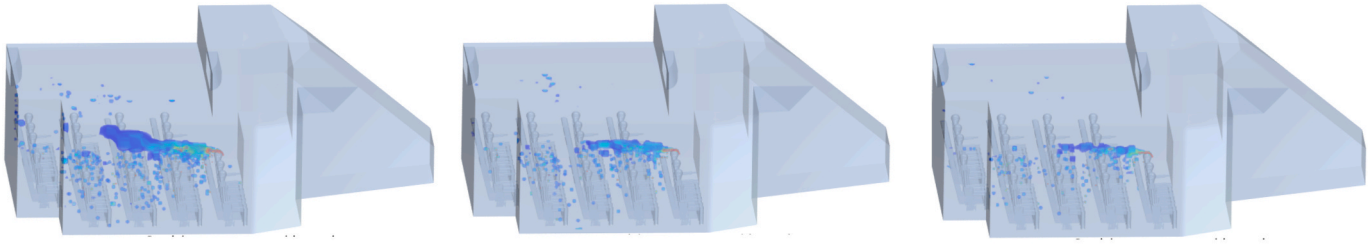

(a) V = 6 knots (b) V = 12 knots (c) V = 18 knots

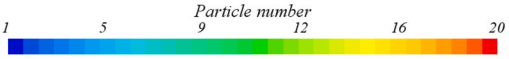

Fig. 14. Comparison of virus distribution for different ship speeds (a front passenger speaking 60 s with the forward door open).

on sea transportation, is looking to recover its crew and passenger operations to aid the economic situation.

(2) The ship's superstructure is compact, and the average voyage time is 12 h, which gives a high-risky environment of COVID-19 transmission where people stay in a crowded space for a fairly long time.

There are two types of virus import mechanisms considered in this work: a passenger coughing and speaking. Both are the most possible initiations of how COVID-19 starts to transmit in such a ship. The virus particle details of coughing and speaking used in this work were set according to the measurements of Chao et al. (2009), as given in Table 1. Coughing is a short event whose duration is considered to be 0.3 s, and speaking is modelled to last 60 s. The viruses injected through coughing have a higher concentration and initial speed than those from speaking, while overall speaking produces more floating viruses as its duration is much longer.

As long as viruses are imported, their transmission relies on airflows. There can be two typical types of airflow in the present case: (a) external airflow comes from the vessel's forward door; (b) internal airflow from ACs. For modelling both the external and internal airflows, the vessel's superstructure was imported into the CFD software at full scale, establishing a computational domain as shown in Fig. 8. The domain was discretised using the fine mesh density as per the reported mesh sensitivity test. CFD investigations were then performed using the approach introduced in Section 2. The COVID-19 transmission due to the two types of airflows was analysed respectively in Sections 4 and 5.

4. External airflow entering the vessel

To study the impact of external airflow entering the vessel on the COVID-19 transmission, the vessel was assumed to advance at a constant speed (V). Four case studies were conducted for V = 6 knots, as a combination of the situations when a passenger sitting in the first row is

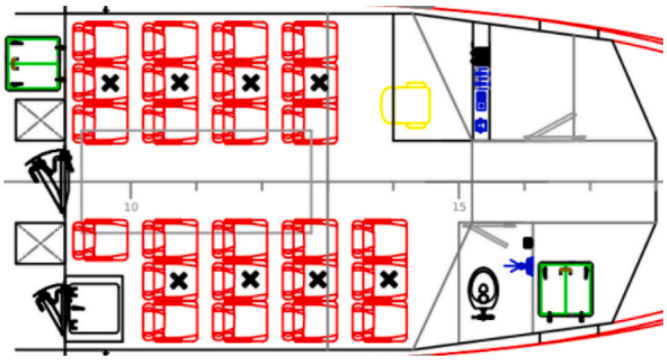

(a) Aligned arrangement

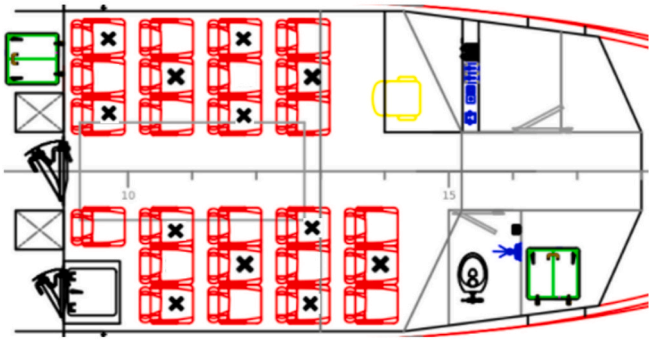

(b) Crossed arrangement (recommended)

Fig. 15. Social distancing for the seat arrangement of the passenger ship – black crosses indicate the seats that should not be used.

coughing or speaking, and when the forward door is open or closed. When the forward door is open, the forward door was set as "fixed-velocity inlet" with a constant velocity of (-V, 0, 0), and the back door was set as "fixed-pressure outlet". Other boundaries were set as "non-slip walls". When the forward door is closed, all boundaries were set as "non-slip walls" and there is no wind flow in the domain.

For the open-door cases, a significant airflow forms inside the vessel. As shown in Fig. 9, this flow takes around 5 s of simulation to converge, thus each of the following simulations was first run for 10 s without particles to ensure the flow convergence. After 10 s, virus particles were injected, assuming from an infected passenger sitting in the first row.

For the simulation of a passenger coughing with the forward door open, it can be seen in Fig. 10 that viruses were coughed out and scattered. Along with the airflow, the viruses moved rapidly towards the back door. For around 5 s, the passengers behind the coughing person were extensively contacted by the viruses, after which the viruses were mostly blown out from the vessel.

For the simulation of a passenger coughing with the forward door closed, it can be seen in Fig. 11 that viruses were coughed out and then only stayed in the area where the passenger sits. The virus movement was mainly a slow sinking due to gravity, alongside a small diffusion due to stochastic motions. Although the viruses stayed in the air for around 100 s, the contagion risk appears to be minimal, based on the assumption that coughing is usually not made directly towards other people.

For the simulation of a passenger speaking with the forward door open, it can be seen in Fig. 12 that a wake of viruses was created and severely affected the passengers behind the speaking person, especially the next two rows. When the speaking stopped, the viruses were carried away from the ship in 10 s.

For the simulation of a passenger speaking with the forward door closed, it can be seen in Fig. 13 that a significant number of viruses were outputted and remained in a small area in front of the speaking person. However, since speaking usually occurs as one person facing another, a

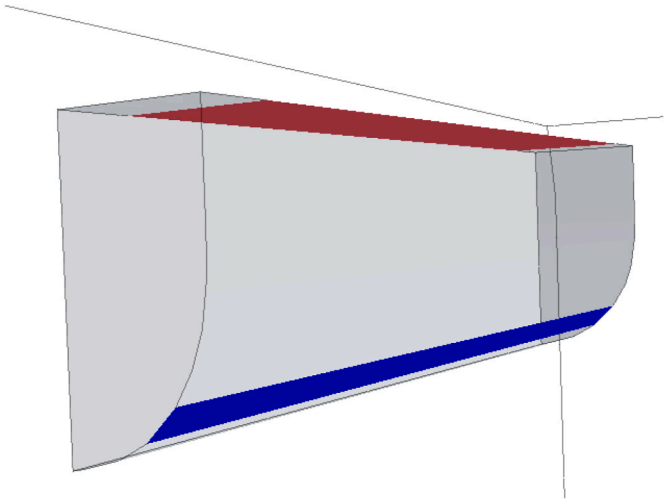

Fig. 17. The air outlet (blue) and return air inlet (red) of the AC. (For interpretation of the references to colour in this figure legend, the reader is referred to the Web version of this article.)

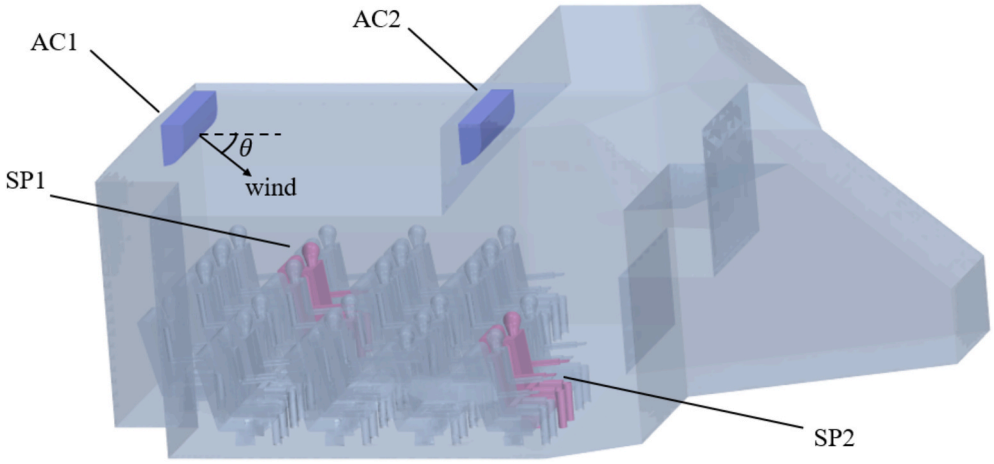

Fig. 16. Illustration of two Air Conditioners (AC1 and AC2) and their corresponding virus import as a nearby speaking person (SP1 and SP2).

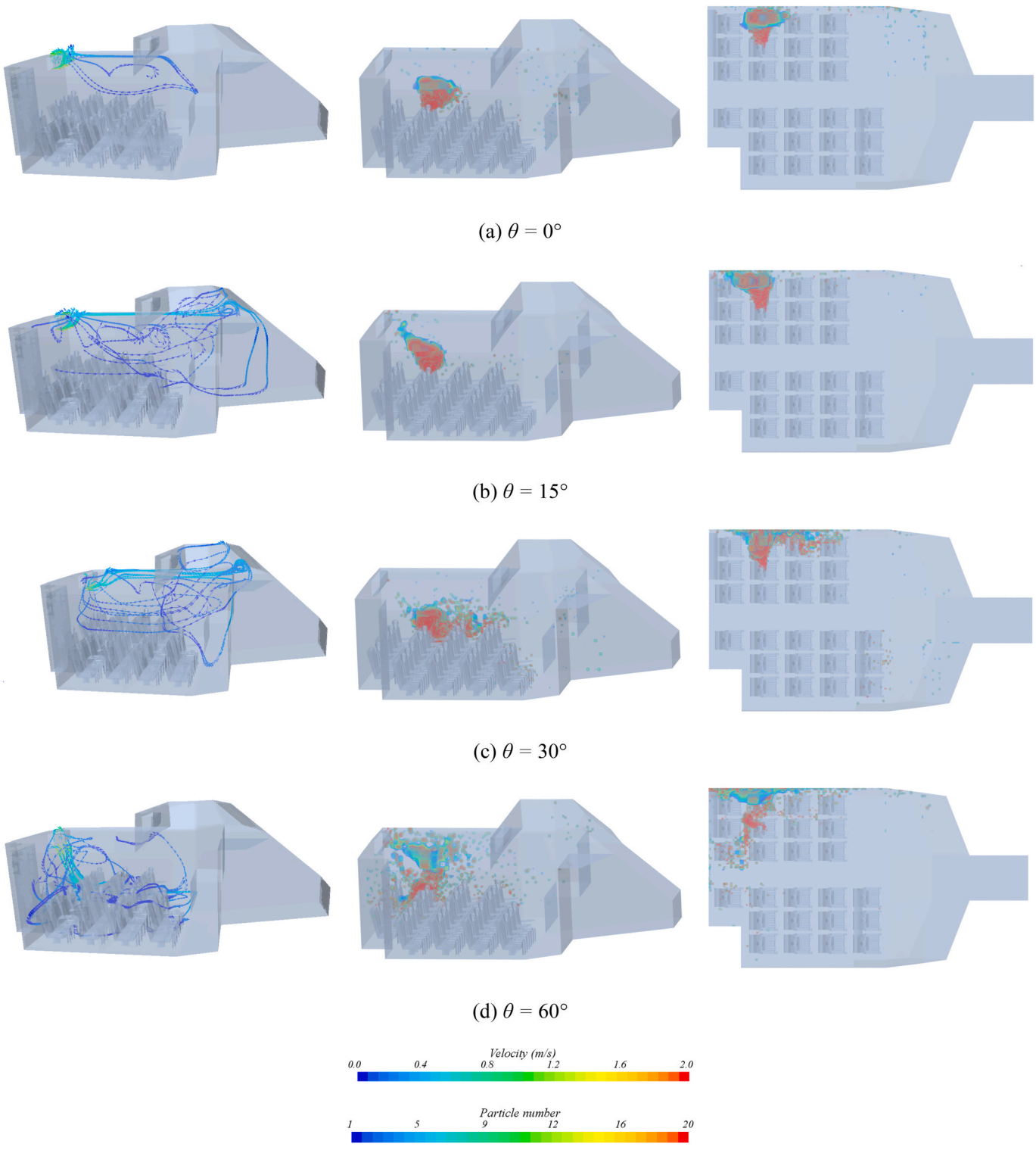

Fig. 18. AC1 wind streamlines and the induced virus distribution.

contagion risk exists if the conversating people are sufficiently close to each other. It is suggested that a safe distance should be half a metre, according to the virus coverage shown in Fig. 13(a). This confirms that it is necessary to keep social distancing in the installed seats.

Combining the results from the four cases, it is shown that: when the ship's forward door is open, a significant airflow forms in the ship, which carries the viruses to make extensive contacts with the passengers in the back seat rows; when the forward door is closed, the viruses mainly sink due to gravity and the diffusion is limited to a small area. These two behaviours are also observed by relevant experimental and computational COVID-19 studies for other environments, as summarised in the review of Katre et al. (2021). More ship speed conditions (V = 12 and 18 knots) have also been tested for the open-door scenario, concerning an infected passenger speaking. It is found that the virus distribution is similar to that of V = 6 knots, despite that the virus spread is smaller when V is higher, as shown in Fig. 14. Overall, it is recommended to keep the forward door closed to minimise the virus's diffusion, although this might be counter-intuitive.

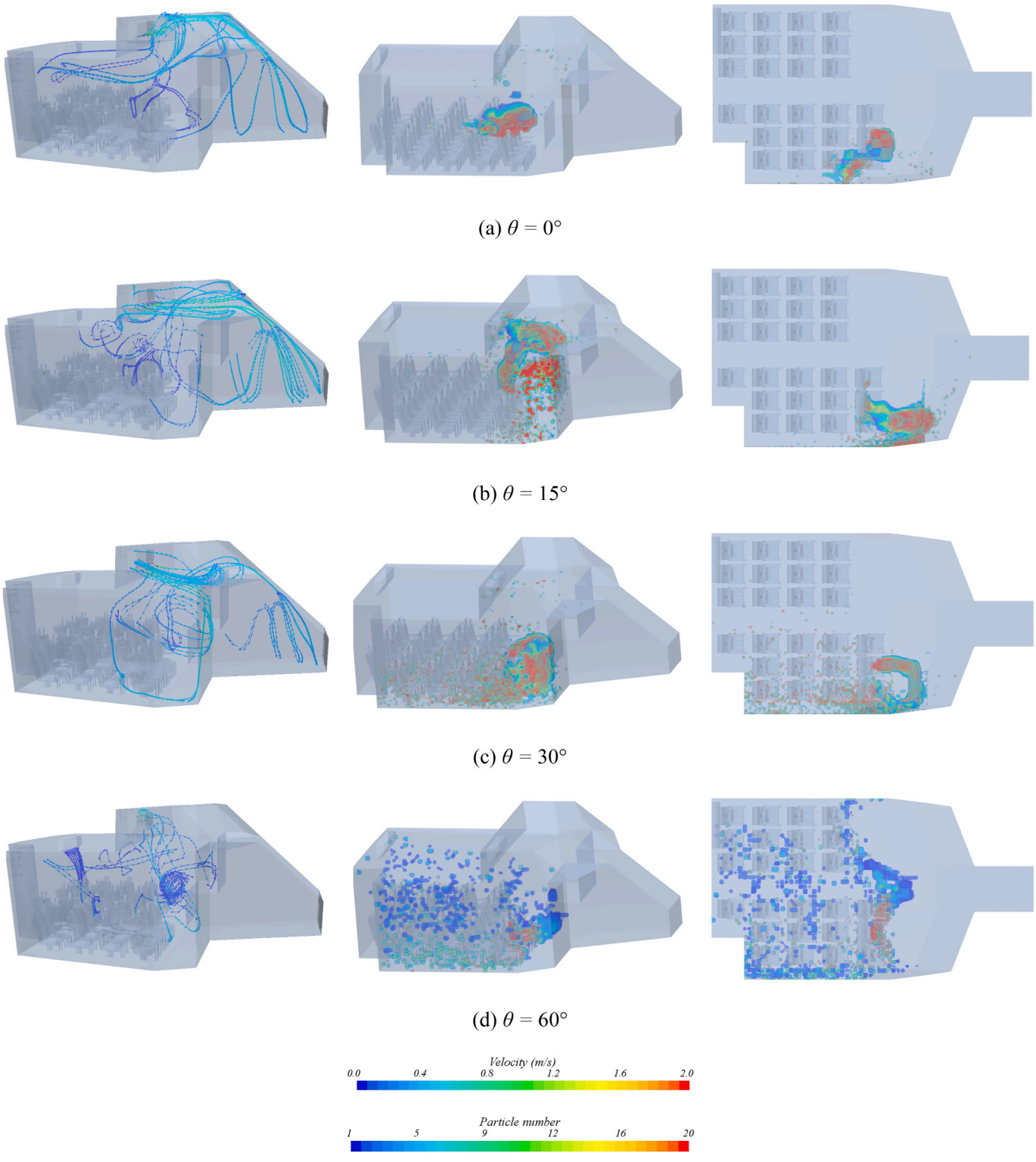

Fig. 19. AC2 wind streamlines and the induced virus distribution.

It is also found that speaking generally creates a higher risk than coughing, as speaking usually lasts a much longer duration, thereby more viruses are introduced to the air. Whilst speaking may have been less altered than coughing which is more likely to be treated as a red flag, the present research suggests that more attention should be paid to the COVID-19 risk in daily conversations.

When there is no external airflow, the modelling indicated that a conversation between two people should keep a distance of at least half a metre (less than a seat's width). Based on this, Fig. 15 presents two potential seat arrangements for the ship. The aligned arrangement shown in Fig. 15(a) reduces the capacity by 33%, and the crossed arrangement shown in Fig. 15(b) reduces the capacity by 50%. However, as the setting in Fig. 15(a) may not avoid the risk from a front passenger who turns around and speaks with the passenger behind, the social distancing setting in Fig. 15(b) is recommended.

5. Internal air conditioner flow

There are two wall-mounted ACs installed inside the ship, respectively in the front and back as shown in Fig. 16 (AC1 and AC2). Each AC has a size of approximately 0.25 m × 1.1 m × 0.45 m, but it is not cubic, as shown in Fig. 17. The AC has an air outlet near the bottom and a return air inlet at the top. The air outlet area is 1.1 m × 0.05 m, and the return air inlet is 0.7 m × 0.25 m. In the CFD model, the AC's outlet was set as "fixed-velocity inlet" with a constant speed of 2 m/s, which was measured on-site when the AC was operating at its middle power. The return air inlet was set as "fixed-velocity outlet" with a constant speed of 0.63 m/s, which was calculated based on volume conservation, i.e. the air amount that exits from the air outlet equals that enters the return air inlet (2 m/s × 1.1 m × 0.05 m ≈ 0.63 m/s × 0.7 m × 0.25).

This study investigates the influence of each AC's airflow direction on the transmission of COVID-19. The airflow direction from the air outlet was varied between 0° and 60° (relative to horizontal, θ), with four cases studied respectively for AC1 and AC2, where $\theta = 0°$, 15°, 30° and 60°. The virus source is assumed as an infected passenger sitting on a seat nearby the opening AC (as marked in Fig. 16), and the person is considered to speak for 60 s.

Figs. 18 and 19 show the velocity field and virus distribution inside the ship, when AC1 or AC2 is operating. It is found that a wall-mounted AC can generate a flow circle that is highly dependent on θ. When θ is 0° or 15°, the AC flow was confined in the top part of the room and within a relatively small region, so did the virus transmission. When θ is 30° or 60°, the virus spread was evidently expanded by the AC flow, which is particularly true for AC2, as shown in Fig. 19(c)&(d). It is also found that an AC tends to accumulate the virus particles, as in both Figs. 18 and 19 where the virus particles gathered near the opening AC. This is because an AC's backflow attracts virus particles to move toward the device.

Based on the findings above, two suggestions are given for the AC operation on such a passenger vessel: (a) control the AC outlet direction at less than 15° downward, and (b) arrange passengers to not sit nearby an operating AC. The second suggestion can be adapted to other AC types whose inlet and outlet are at separate locations in a room (such as the setup in Fig. 1), and the suggestion is to not sit downstream of the AC flow.

6. Conclusions

To provide effective measures that can minimise COVID-19 transmission for passenger vessels, a computational model has been established to investigate the airborne transmission of the virus in the superstructure of a small passenger vessel. The model was validated against experimental results to prove the capability of accurately predicting the velocity field and virus distribution inside a room. Based on the validated model, a series of simulations were conducted to study the influence on the virus transmission from both external wind flow and internal AC flow. The simulation results have helped identify operational improvements as summarised below.

When the forward door is open, ship advancement generates an extensive wind flow across the passenger area, which fosters the spread of virus. Therefore, it is suggested to keep the ship's forward door shut. When there is no wind flow in the vessel's superstructure, the virus spread from coughing or speaking is limited to a radius of half a metre. Based on the radius, a crossed seat arrangement plan has been proposed in the present paper.

Although wall-mounted ACs could also foster the spread of virus in a vessel, this study has demonstrated that this effect can be suppressed by controlling the AC outlet direction to be less than 15° downward. In addition, it is found that virus particles can follow an AC's backflow to accumulate. Hence, sitting far from an opening wall-mounted AC can minimise the associated risk.

In future work, the computational approach can be applied to study the COVID-19 airborne transmission in other environments. Many maritime environments are still at COVID-19 risk which requires more research, such as a large cruise ship, an open-air finishing vessel and an offshore platform.

CRediT authorship contribution statement

Luofeng Huang: Conceptualization, Methodology, Software, Validation, Visualization, Investigation, Writing – original draft. **Soegeng Riyadi:** ConceptualizationConceptualisation, Investigation, Resources. **I.K.A.P. Utama:** Supervision, Project administration, Funding acquisition, Writing – review & editing. **Minghao Li:** Methodology, Software, Visualization. **Peiyign Sun:** Software, Investigation. **Giles Thomas:** Supervision, Project administration, Funding acquisition, Writing – review & editing.

Declaration of competing interest

The authors declare that they have no known competing financial interests or personal relationships that could have appeared to influence the work reported in this paper.

Acknowledgements

This work is part of a project that has received funding from the British Council under the Newton Institutional Links Grants - Ensuring the safety of Indonesian seafarers and fishers in the time of COVID-19 and beyond (agreement No. 623457938), in conjunction with the Indonesian Governmental Funding from the Ministry of Education, Culture, and Higher Education (agreement No. 2242/PKS/ITS/2021). The authors appreciate PT. Pelayaran Nasional Ekalya Purnamasari (PNEP) for sharing the studied vessel's geometry and information.

Appendix A. Numerical uncertainty analysis

The approximation of a physical problem via CFD requires the solution of a set of partial differential equations, as introduced in Section 2. Due to a lack of closed-form solutions for the RANS equations, the present work discretised the governing equations in space and obtained approximate results. Thus the discretisation resolution, i.e. mesh density, has a significant impact on the prediction. In order to assess the associated uncertainty, here applies the GCI method (Celik et al., 2008).

Step 1 :

Defined three mesh densities $h_1 = 0.03$ m, $h_2 = 0.04$ m, $h_5 = 0.05$ m.

Step 2 :

Calculated $r_{21} = h_2/h_1 = 1.33$, and $r_{32} = h_3/h_2 = 1.25$.

A variable critical φ was defined as velocity magnitude at the central point of the room (Fig. 2).
Calculated:

$$P = \frac{1}{\ln(r_{21})}\left|ln\left|\varepsilon_{32}/\varepsilon_{21}\right| + q(P)\right|$$

$$q(P) = \ln\left(\frac{r_{21}^{P} - S}{r_{32}^{P} - S}\right)$$

$$S = 1 \cdot sgn(\varepsilon_{32} / \varepsilon_{21})$$

where $\varepsilon_{32} = \varphi_3 - \varphi_2$, $\varepsilon_{21} = \varphi_2 - \varphi_1$.

Step 4 :

Calculated the extrapolated value:

$$\varphi_{ext}^{21} = \left|r_{21}^{P}\ \varphi_1 - \varphi_2\right| / \left(r_{21}^{P} - 1\right)$$

Step 5 :

Calculated the approximate relative error:

$$e_a^{21} = \left|\frac{\varphi_1 - \varphi_2}{\varphi_1}\right|$$

Calculated extrapolated relative error:

$$e_{ext}^{21} = \left|\frac{\varphi_{ext}^{21} - \varphi_1}{\varphi_{ext}^{21}}\right|$$

Calculated the fine-grid convergence index:

$$GCI_{fine}^{21} = \frac{1.25 e_a^{21}}{r_{21}^{P} - 1}$$

The results are summarised in Table A1, in which the numerical uncertainty in the fine-mesh solution for the velocity magnitude is 3.68%

Table A1
calculations of spatial discretisation uncertainty

Parameter	Value
r_{21}	1.33
r_{32}	1.25
φ_1	0.0163
φ_2	0.0175
φ_3	0.0203
P	4.3967
φ_{ext}^{21}	0.0158
e_a^{21}	7.36%
e_{ext}^{21}	2.94%
GCI_{fine}^{21}	3.68%

References

Abuhegazy, M., Talaat, K., Anderoglu, O., Poroseva, S.V., 2020. Numerical investigation of aerosol transport in a classroom with relevance to COVID-19. Phys. Fluids 32, 103311.

Celik, I.B., Ghia, U., Roache, P.J., Freitas, C.J., 2008. Procedure for estimation and reporting of uncertainty due to discretization in CFD applications. J. Fluids Eng. Transact. ASME 130.

Chao, C.Y.H., Wan, M.P., Morawska, L., Johnson, G.R., Ristovski, Z.D., Hargreaves, M., Mengersen, K., Corbett, S., Li, Y., Xie, X., 2009. Characterization of expiration air jets and droplet size distributions immediately at the mouth opening. J. Aerosol Sci. 40, 122–133.

Chen, F., Simon, C.M., Lai, A.C., 2006. Modeling particle distribution and deposition in indoor environments with a new drift–flux model. Atmos. Environ. 40, 357–367.

Gao, N.P., Niu, J.L., 2007. Modeling particle dispersion and deposition in indoor environments. Atmos. Environ. 41, 3862–3876.

Gosman, A.D., Loannides, E., 1983. Aspects of computer simulation of liquid-fueled combustors. J. Energy 7, 482–490.

Guo, L., Torii, R., Epstein, R., Rubin, J., Reid, J.P., Li, H., Ducci, A., Balachandran, R., Tiwari, M.K., Ventikos, Y., Lovat, L.B., 2021. Using portable air purifiers to reduce airborne transmission of infectious respiratory viruses – a computational fluid dynamics study. medRxiv. https://doi.org/10.1101/2021.11.01.21265775, 11.01.21265775, 2021.

Huang, L., Tuhkuri, J., Igrec, B., Li, M., Stagonas, D., Toffoli, A., Cardiff, P., Thomas, G., 2020. Ship resistance when operating in floating ice floes: a combined CFD&DEM approach. Mar. Struct. 74, 102817.

Jin, Y., Yang, H., Ji, W., Wu, W., Chen, S., Zhang, W., Duan, G., 2020. Virology, epidemiology, pathogenesis, and control of COVID-19. Viruses 12, 372.

Katre, P., Banerjee, S., Balusamy, S., Sahu, K.C., 2021. Fluid dynamics of respiratory droplets in the context of COVID-19: airborne and surfaceborne transmissions. Phys. Fluids 33, 081302.

Liu, A.B., Mather, D., Reitz, R.D., 1993. Modeling the effects of drop drag and breakup on fuel sprays. SAE Trans. 83–95.

Menter, F., 1993. Zonal two equation kw turbulence models for aerodynamic flows, in: 23rd Fluid Dynamics. In: Plasmadynamics, and Lasers Conference, p. 2906.

Millefiori, L.M., Braca, P., Zissis, D., Spiliopoulos, G., Marano, S., Willett, P.K., Carniel, S., 2021. COVID-19 impact on global maritime mobility. Sci. Rep. 11, 18039 https://doi.org/10.1038/s41598-021-97461-7.

Pena, B., Huang, L., 2021. A review on the turbulence modelling strategy for ship hydrodynamic simulations. Ocean Eng. 241, 110082.

Talaat, K., Abuhegazy, M., Mahfoze, O.A., Anderoglu, O., Poroseva, S.V., 2021. Simulation of aerosol transmission on a Boeing 737 airplane with intervention measures for COVID-19 mitigation. Phys. Fluids 33, 033312.

Thomas, G., Huang, L., Ryan, C., Utama, I., Riyadi, S., Setyawan, D., Hetharia, W., 2021. Safer onboard environments for Indonesian seafarers and Fishers in the time of COVID-19 and beyond. In: International Conference on Ship and Offshore Technology. The Royal Institution of Naval Architects (RINA), Surabaya, Indonesia.

Vuorinen, V., Aarnio, M., Alava, M., Alopaeus, V., Atanasova, N., Auvinen, M., Balasubramanian, N., Bordbar, H., Erästö, P., Grande, R., 2020. Modelling aerosol transport and virus exposure with numerical simulations in relation to SARS-CoV-2 transmission by inhalation indoors. Saf. Sci. 130, 104866.

Welch, D., Buonanno, M., Buchan, A.G., Yang, L., Atkinson, K.D., Shuryak, I., Brenner, D. J., 2022. Inactivation rates for airborne human coronavirus by low doses of 222 nm far-UVC radiation. Viruses 14, 684.

Zhang, Z., Capecelatro, J., Maki, K., 2021a. On the utility of a well-mixed model for predicting disease transmission on an urban bus. AIP Adv. 11, 085229.

Zhang, Z., Han, T., Yoo, K.H., Capecelatro, J., Boehman, A.L., Maki, K., 2021b. Disease transmission through expiratory aerosols on an urban bus. Phys. Fluids 33, 015116.